Image Mosaic Based on Improved Logarithmic Polar Coordinate Transformation and Ransac Algorithm

Dan Li, Lei Chen(✉), Jun Tian, Dai-hong Jiang, Jin-ping Sun, and Bin Ding

Key Laboratory of Intelligent Industrial Control Technology of Jiangsu Province, Xuzhou University of Technology, Xuzhou 221000, Jiangsu, China
lidanonline@163.com, chenlei@xzit.edu.cn

Abstract. Complex factors with the electronic noise, X-ray scattering and uneven illumination often disturb the image registration. A new algorithm was proposed in this paper. The improved phase correlation algorithm based on log polar transformation was used to calculate parameters, such as rotation, scaling and translation. Then, the Harris corner matching points were extracted in overlapping positions and purified by the improved Ransac algorithm. Finally, images were processed by NSCT transform algorithm to make the image joint seemed smooth and natural. Experiments confirmed that, the new algorithm is accurate and efficient, and has high robustness to complex environment.

Keywords: Image registration · Logarithmic polar coordinates · Mosaic · Ransac algorithm · NSCT transform

1 Introduction

In medical images, panoramic image equipment is very expensive and the visual field of most medical imaging devices is limited [1]. Using image stitching technology [2–4] to generate panoramic images has low cost and good effect, but under the influence of complex factors, the result details are blurred. With the development of computer and multimedia technology, the requirement of real-time network transmission of mosaic video images is becoming higher and higher [5–7].

In view of the above problems, a new image registration and stitching algorithm was proposed. First, using the improved phase correlation algorithm of logarithmic polar coordinate transformation to calculate the parameters of scaling, rotation and translation, and estimate the overlapped region. Then, the Harris corner points were extracted and the Ransac algorithm [8, 9] was improved to accurately purify the matching points. Finally, the NSCT transformation algorithm [10] was used and the fusion strategy was formulated to further solve the splicing joint.

H. Song et al. (Eds.): SIMUtools 2019, LNICST 295, pp. 608–614, 2019.
https://doi.org/10.1007/978-3-030-32216-8_59

2 Improvement of Logarithmic Polar Coordinate

In order to improve the robustness of different environments, this paper uses the polar coordinate transformation to improve the phase correlation algorithm, which can adapt to the situation of rotation, scaling and displacement.
Step 1: The image $I_1(x, y)$ and $I_2(x, y)$ are converted to $I_1'(u, v)$ after Fourier transform. When I_1 and I_2 exist translation, rotation, and scaling, the relationship is:

$$I_2(x, y) = I_1(\lambda x\cos\theta_0 + \lambda y\sin\theta_0 - \Delta x, -\lambda x\sin\theta_0 + \lambda y\text{cons}\theta_0 - \Delta y) \tag{1}$$

λ is scaling ratio, θ_0 is rotation angle, and Δx and Δy are translation distances.

$$I_2'(u, v) = \frac{e^{-j2\pi(u\Delta x + v\Delta y)}}{\lambda^2} I_1'((u\cos\theta_0 + v\sin\theta_0)/\lambda, (-u\sin\theta_0 + v\cos\theta_0)/\lambda) \tag{2}$$

Step 2: $\rho = \sqrt{u^2 + v^2}$, $\theta = \arctan(u/v)$, transform the space of the image to the logarithmic polar space:

$$\left|I_2'(\rho\cos\theta, \rho\sin\theta)\right| = \left|I_1'(\rho\cos(\theta - \theta_0)/\lambda, \rho\sin(\theta - \theta_0)/\lambda)\right| \tag{3}$$

Step 3: $\eta = \log\rho$, $\eta_0 = \log\lambda$, M_1 and M_2 are the models of I_1' and I_2', $M_2(\eta, \theta) = M_1(\eta - \eta_0, \theta - \theta_0)$. The conjugate power spectrum of $M_2(u, v)$ is $M_2^*(u, v)$. After normalization, the cross power spectrum of the image is expressed as follows:

$$\frac{M_1(u, v)M_2^*(u, v)}{\left|M_1(u, v)M_2^*(u, v)\right|} = e^{-j2\pi(u\eta_0 + v\theta_0)} \tag{4}$$

Step 4: After the inverse Fourier transform, the impulse function is obtained.

$$F^{-1}[e^{-j2\pi(u\eta_0 + v\theta_0)}] = \delta(\eta - \eta_0, \theta - \theta_0) \tag{5}$$

The position of the peak of impulse function means the size of the scaling ratio λ and the angle θ_0 of rotation. Inverse transform I_2 according to the scaling ratio and the rotation angle, then the translation distance $(\Delta x, \Delta y)$ is calculated with I_1 by the phase correlation method.

3 Registration and Feature Purification

3.1 Corner Extraction

The Harris algorithm detects the corner points by the change of the gray level after moving the local sliding window. Make $I(x, y)$ a gray value at (x, y), $w(x, y)$ is a Gauss filter, and the horizontal vertical position of the window is u and v. $E(u, v)$ is an autocorrelation function in any direction, that is the sum of gray scale error in the window. The expressions of $E(u, v)$ and $w(x, y)$ are as follows:

$$E(u,v)=\sum_{x,y} w(x,y)[I(x+u,y+v)-I(x,y)]^2 \quad w(x,y)=\frac{1}{2\pi\sigma^2}e^{-\frac{(x^2+y^2)}{2\sigma^2}} \tag{6}$$

The Gauss window function $w(x,y)$ increases the weight of pixels near the center point. $I(x+u,y+v)-I(x,y)$ is the gradient of the image, σ is the standard deviation. After the formula (6) is carried out by Taylor's expansion and neglecting the high term, the matrix form of $E(u,v)$ and M are as follows.

$$E(u,v)\cong[u,v]M\begin{bmatrix}u\\v\end{bmatrix} \quad M=\sum_{x,y} w(x,y)\begin{bmatrix}I_x^2 & I_xI_y\\ I_xI_y & I_y^2\end{bmatrix}=w(x,y)*\begin{bmatrix}I_x^2 & I_xI_y\\ I_xI_y & I_y^2\end{bmatrix} \tag{7}$$

I_x and I_y are the partial derivatives of the x,y. $A=I_x^2*w$, $B=I_y^2*w$, $C=(I_xI_y)*w$, the corner response function is shown by the following formula.

$$R=\det\ M-k(\mathrm{tr}\,M)^2=(AB-C^2)^2-k(A+B)^2 \tag{8}$$

The σ_D and $s\sigma_D$ are the scale space integral and the differential factor respectively and matrix M is expressed as:

$$M=s\sigma_D^2 w(x,y,\sigma_D)*\begin{bmatrix}I_x^2(x,y,s\sigma_D) & I_x(x,y,s\sigma_D)I_y(x,y,s\sigma_D)\\ I_x(x,y,s\sigma_D)I_y(x,y,s\sigma_D) & I_y^2(x,y,s\sigma_D)\end{bmatrix} \tag{9}$$

3.2 Feature Registration

After the corner points are extracted, the feature matching is performed by the normalized cross correlation coefficient. The feature point is centered in a square window ω. The NCC value as a matching principle. $\bar{I}_1$ and $\bar{I}_2$ are the mean value of the gray level of the square window pixels to be matched. When the matching method based on NCC is affected by illumination, scale transformation and noise, the matching accuracy is reduced. Window size is $(2N+1)\times(2N+1)$. $\bar{I}_1$, $\bar{I}_2$ and NCC are expressed as follows:

$$\begin{aligned}\bar{I}_1&=\frac{1}{(2N+1)^2}\sum_{x,y\in\omega} I_1(x,y)\\ \bar{I}_2&=\frac{1}{(2N+1)^2}\sum_{x,y\in\omega} I_2(x,y)\\ NCC&=\frac{\sum_{x,y\in\omega}[I_1(x,y)-\bar{I}_1][I_2(x,y)-\bar{I}_2]}{\sqrt{\sum_{x,y\in\omega}[I_1(x,y)-\bar{I}_1]^2}\sqrt{\sum_{x,y\in\omega}[I_2(x,y)-\bar{I}_2]^2}}\end{aligned} \tag{10}$$

3.3 Ransac Algorithm Improvement and Splicing

In order to reduce error matching, an improved Ransac algorithm can eliminate the mismatch feature points. Nine matching points are more convenient to verify the temporary model, it can timely re-select the random sample set.

The maximum and minimum of the coordinates of the matching points are selected from the reference image I_1. The matching feature points are divided into M*M blocks. This paple takes $M = 6$. Randomly select 9 different blocks in the I_1 and randomly select a matching point from each of the 9 blocks to constitute the sample set with 9 corresponding matching points in image I_2. As shown in the following formula, $h_{11}, \ldots, h_{32}$ are degree of freedom.

$$\begin{bmatrix} x \\ y \\ 1 \end{bmatrix} = h \begin{bmatrix} x' \\ y' \\ 1 \end{bmatrix} = \begin{bmatrix} h_{11} & h_{12} & h_{13} \\ h_{21} & h_{22} & h_{23} \\ h_{31} & h_{32} & 1 \end{bmatrix} \begin{bmatrix} x' \\ y' \\ 1 \end{bmatrix} \tag{11}$$

Check whether ninth pairs of matching points are support sets for the basic matrix of the temporary model, if not, 9 pairs of matching points are re-selected. Repeat the Step 2, if it is the support set, the temporary model matrix h is considered as a candidate matrix h. Iteratively calculates the minimum value of the error function E of the matching point pairs, and updates the matrix h, $E = \sum_{i=1}^{P} e_i^2 = \sum_{i=1}^{P} [I_2(x_i', y_i') - I_1(x_i, y_i)]^2$.

3.4 Image Fusion

The NSCT algorithm is composed of non sampling Pyramid and non sampling directional filters. While maintaining the translation invariance, it has good direction selectivity, time frequency localization, and multi-resolution characteristics.

Step 1: Suppose $A(x, y)$ and $B(x, y)$ are the overlapped regions. After multiscale decomposition, it can get a series of subband A_l^k and B_l^k, l = 1, 2, 3, …, L, L is the largest number of layers of decomposition.

Step 2: For the low frequency subband, the image change is slow, and the direct average fusion method is used, $AB_L^0 = (A_L^0 + B_L^0)/2$.

Step 3: For the high frequency sub-band, it reflects the sensitive edges and details of the human eye. Using high frequency subband weighted fusion method based on regional variance saliency. As shown in formula (12):

$$AB_l^k(x, y) = \begin{cases} \begin{cases} (1-w)A_l^k + wB_l^k & G(A) \geq G(B) \\ wA_l^k + (1-w)B_l^k & G(A) < G(B) \end{cases} & M \geq T \\ \begin{cases} A_l^k & G(A) \geq G(B) \\ B_l^k & G(A) < G(B) \end{cases} & M < T \end{cases} \tag{12}$$

$$w = 0.5 - 0.5\left(\frac{1-M}{1-T}\right)$$

Step 4: Reconstructed image and output fused image.

4 Experimental Results and Analysis Conclusion

As shown in Fig. 1(f)–(h) are the energy distributions of (a) (b), (a) (c), (a) (d) impulse function respectively. According to the information of large peak parameters, the location of overlapping regions is roughly estimated to reduce the extraction range of feature points in precise registration. Because there is no overlap area in (a) (e), so there is no maximum prominence peak in (i).

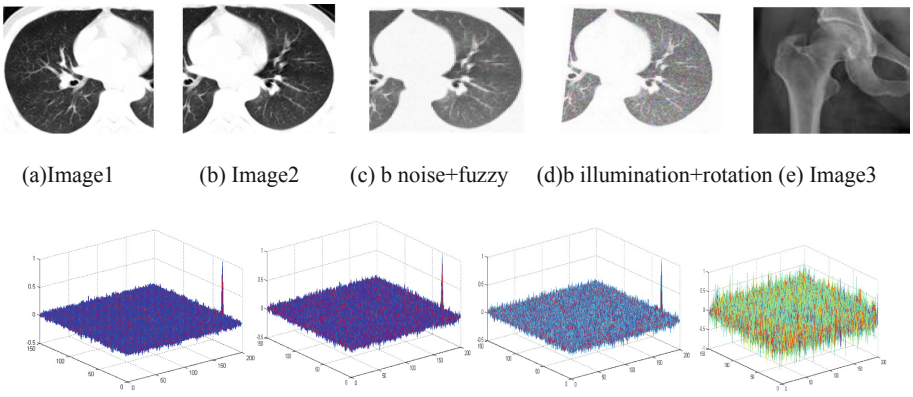

(a)Image1 (b) Image2 (c) b noise+fuzzy (d)b illumination+rotation (e) Image3

(f)ab impulse function (g)ac impulse function (h)ad impulse function (i)ae impulse function

Fig. 1. Distribution of impulse function

Figure 2 compares the NCC matching method with the new method. (a) is the result of NCC matching, threshold selection is 0.6. Because of the low resolution, there are a lot of mismatching points. (b) is the result of the improved Ransac algorithm in this paper, the mismatch was removed. (c)–(g) are the matching results under the changes of scaling, noise, rotation, brightness and perspective transformation. (h) is the result of mixing the scaling, rotation and the perspective transformation.

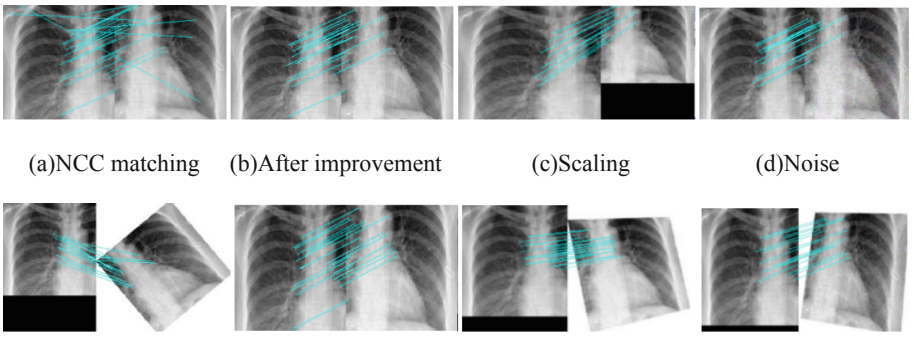

(a)NCC matching (b)After improvement (c)Scaling (d)Noise

(e)Rotation (f)Brightness (g)Perspective (h)Mixed

Fig. 2. Image registration

Table 1 is the transformation matrix and corners information of the Fig. 2(c)–(h). The table sets up the parameter values of the degree of freedom for the matrix H between images, and describes the number of points in the image and the number of the matched corners.

Table 1. Corner registration and transformation matrix

	Scaling			Noise			Rotation		
H	1.4396	−0.0363	75.5787	0.9102	−0.0404	75.4524	0.8076	−0.6124	34.1210
	−0.0279	1.4439	33.8658	−0.0323	0.9288	34.2291	0.6703	0.7795	−41.4569
	−0.0004	−0.0004	1.0000	−0.0005	−0.0005	1.0000	0.0001	0.0002	1.0000
Right image	64			117			168		
Matching points	16			18			15		
	Brightness			Perspective			Mixed		
H	0.9666	0.0003	75.2576	0.7379	−0.1229	80.2946	1.1633	0.3355	44.1548
	−0.0203	0.9974	33.2290	−0.0477	1.1097	6.3354	−0.0723	1.2982	21.4007
	−0.0002	0.0000	1.0000	−0.0018	0.0009	1.0000	−0.0001	0.0013	1.0000
Right image	107			176			147		
Matching points	22			16			15		

Figures 3 and 4 are the comparison of stitching results, (a) is a image of before stitching. (b)–(d) are the results of direct stitching, average gradient stitching and new method stitching. After the fusion and reconstruction of the decomposed low frequency and high frequency subbands, (d) shows the image joint is more smooth and more clear.

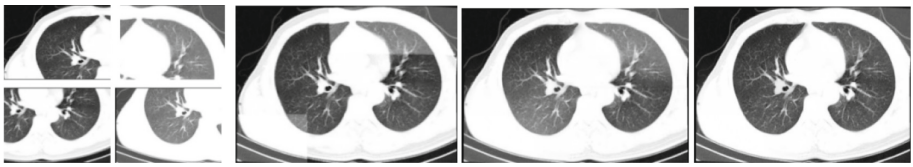

(a) Before stitching (b) Direct (c) Average gradient (d) This paper

Fig. 3. Comparison of lungs stitching results

(a) Before stitching (b) Direct (c) Average gradient (d) This paper

Fig. 4. Comparison of hip stitching results

5 Conclusion

The new algorithm improves the phase correlation algorithm by using the logarithmic polar coordinate transformation, so that it can adapt to the situation of scaling, rotation and translation between the images adaptively. After using NCC normalized cross-correlation coefficient to extract Harris corners at overlapping positions, the improved Ransac algorithm is used to precisely purify, optimize model parameters. In the mosaic process, we use NSCT transform algorithm to design fusion strategy, which solves the problem of noise accuracy, low resolution and low contrast interference and saves the cost of medical equipment.

Acknowledgements. This work is partly supported by the Key Laboratory of Intelligent Industrial Control Technology of Jiangsu Province Research Project(JSKLIIC201705), Xuzhou Science and Technology Plan Projects (KC18011, KC16SH010, KC17078), Major Project of Natural Science Research of the Jiangsu Higher Education Institutions of China (18KJA520012), Ministry of Housing and Urban-Rural Development Science and Technology Planning Project (2016-R2-060).

References

1. Menon, H.P.: Issues involved in automatic selection and intensity based matching of feature points for MLS registration of medical images. In: International Conference on Advances in Computing, Communications and Informatics, pp. 787–792 (2017)
2. Jia, J., Tang, C.K.: Image stitching using structure deformation. IEEE Trans. Pattern Anal. Mach. Intell. **34**(4), 617–631 (2008)
3. Zhang, F., Liu, F.: Parallax-tolerant image stitching. In: Computer Vision and Pattern Recognition, pp. 3262–3269 (2014)
4. Chia, W.C., Chew, L.W., Ang, L.M., et al.: Low memory image stitching and compression for WMSN using strip-based processing. Int. J. Sens. Netw. **11**(1), 22–32 (2012)
5. Jiang, D., Wang, W., Shi, L., Song, H.: A compressive sensing-based approach to end-to-end network traffic reconstruction. IEEE Trans. Netw. Sci. Eng. (2018). https://doi.org/10.1109/tnse.2018.2877597
6. Jiang, D., Huo, L., Song, H.: Rethinking behaviors and activities of base stations in mobile cellular networks based on big data analysis. IEEE Trans. Netw. Sci. Eng. **1**(1), 1–12 (2018)
7. Jiang, D., Han, Y., Miao, L., et al.: Dynamic access approach to multiple channels in pervasive wireless multimedia communications for technology enhanced learning. J. Intell. Fuzzy Syst. **31**(5), 2497–2509 (2016)
8. El-Melegy, M.T.: RANSAC algorithm with sequential probability ratio test for robust training of feed-forward neural networks. In: International Joint Conference on Neural Networks, vol. 3, no. 14, pp. 3256–3263 (2011)
9. Olofsson, K., Holmgren, J.: Tree stem and height measurements using terrestrial laser scanning and the RANSAC algorithm. Remote Sens. **6**(5), 4323–4344 (2014)
10. Yang, Y., Tong, S., Huang, S., et al.: Multifocus image fusion based on NSCT and focused area detection. IEEE Sens. J. **15**(5), 2824–2838 (2015)